Int. J. Solids Structures Vol. 17, No. 11, 1037–1042, 1981
Printed in Great Britain.

0020-7683/81/111037-06$02.00/0
Pergamon Press Ltd.

IMPACT RESPONSE OF A PENNY-SHAPED CRACK PLACED PARALLEL TO THE BOUNDARY OF AN INFINITE SLAB†

R. B. MOHAPATRA and H. PARHI
Department of Mathematics, Regional Engineering College, Rourkela-769008, India

(*Received* 25 *July* 1980; *in revised form* 3 *December* 1980)

Abstract—The axisymmetric dynamical problem is presented for an infinite slab weakened by a penny-shaped crack. The crack is assumed to be opened by the application of a step stress. Laplace and Henkel transform techniques are used to reduce the probelm to the solution of a Fredholm integral equation of the second kind in a transformed plane. Finally the problem is solved by a special numerical Laplace inversion technique. Numerical results on the dynamic stress-intensity factor are obtained. The influence of inertia, finite boundaries and their interactions on the load transfer to the crack are considered.

1. INTRODUCTION

In fracture mechanics, it is important to reveal the behaviour of dynamic stresses in the vicinity of crack or cracks. The dynamic response of a penny-shaped crack under the action of impact loads in specimens having large dimensions has been treated by many authors[1–3]. In above papers the effect of boundary is neglected in the analysis. In presence of finite boundaries the problem becomes more complicated due to interaction between the scattered waves from the crack edge and the reflected waves from the boundaries. Recently Chen[4] has solved the problem of elastodynamic response of a penny-shaped crack in an infinite cylinder of finite radius.

In this paper we present the solution of the impact load on a penny-shaped crack placed parallel at the centre of an elastic slab. Two cases are considered (i) the boundary is stress free (ii) the slab is confined between two rigid planes. For each of these cases, using Laplace and Hankel transforms we reduce the problem to the solution of a pair of integral equations and finally to a Fredholm integral equation of the second kind in the Laplace transformed plane. To recover the time dependent solution a numerical technique used by Miller and Guy is adopted. Finally the dynamic stress-intensity factor is calculated. The influence of inertia, geometry and their interactions are shown graphically.

2. FORMULATION OF THE PROBLEM

We consider an infinite slab of thickness "$2b$" containing a centrally placed penny-shaped crack of radius "a". The impact of load is applied symmetrically about z-axis through which the penny-shaped crack is centered. The axi-symmetric displacements and stresses can be derived from two potential functions $\phi(\gamma, z, t)$ and $\psi(\gamma, z, t)$ as

$$u_\gamma(\gamma, z, t) = \frac{\partial \phi}{\partial \gamma} - \frac{\partial \psi}{\partial z}, \qquad u_z(\gamma, z, t) = \frac{\partial \phi}{\partial z} + \frac{\partial \psi}{\partial \gamma} + \frac{\psi}{\gamma} \tag{1}$$

$$\sigma_\gamma(\gamma, z, t) = 2\mu \frac{\partial}{\partial \gamma}\left(\frac{\partial \phi}{\partial \gamma} - \frac{\partial \psi}{\partial z}\right) + \lambda \nabla^2 \phi$$

$$\sigma_\theta(\gamma, z, t) = \frac{2\mu}{\gamma}\left(\frac{\partial \phi}{\partial \gamma} - \frac{\partial \psi}{\partial z}\right) + \lambda \nabla^2 \phi \tag{2}$$

$$\sigma_z(\gamma, z, t) = 2\mu \frac{\partial}{\partial z}\left(\frac{\partial \phi}{\partial z} + \frac{\partial \psi}{\partial \gamma} + \frac{\psi}{\gamma}\right) + \lambda \nabla^2 \phi$$

$$\tau_{\gamma z}(\gamma, z, t) = \mu\left[\frac{\partial}{\partial z}\left(2\frac{\partial \phi}{\partial \gamma} - \frac{\partial \psi}{\partial z}\right) + \frac{\partial}{\partial \gamma}\left(\frac{\partial \psi}{\partial \gamma} + \frac{\psi}{\gamma}\right)\right]$$

$$\tau_{\gamma\theta} = \tau_{\theta z} = 0 \tag{3}$$

†This work is supported by the Council of Scientific and Industrial Research, India.

where

$$\nabla^2 = \frac{\partial^2}{\partial \gamma^2} + \frac{1}{\gamma}\frac{\partial}{\partial \gamma} + \frac{\partial^2}{\partial z^2}.$$

It can easily be shown that the equations of motions are satisfied if ϕ and ψ are governed by the wave equations

$$\nabla^2 \phi = \frac{1}{c_1^2}\frac{\partial^2 \phi}{\partial t^2}$$

$$\nabla^2 \psi - \frac{\psi}{\gamma^2} = \frac{1}{c_2^2}\frac{\partial^2 \psi}{\partial t^2} \tag{4}$$

where

$$c_1 = \left(\frac{\lambda + 2\mu}{\rho}\right)^{1/2}, \qquad c_2 = \left(\frac{\mu}{\rho}\right)^{1/2}$$

ρ, being the mass density of the elastic material. The problem of finding the distribution of stresses in the vicinity of the crack is equivalent to that of finding the distribution of stresses in $0 \leqslant z \leqslant b$, $a \leqslant \gamma < \infty$ when its plane boundary $z = 0$ is subjected to following conditions

$$\sigma_z(\gamma, 0, t) = -\sigma_0 H(t), \qquad 0 \leqslant \gamma < a \tag{5}$$

$$u_z(\gamma, 0, t) = 0, \qquad a < \gamma < \infty \tag{6}$$

$$\tau_{\gamma z}(\gamma, 0, t) = 0, \qquad \forall \gamma. \tag{7}$$

For the boundary $z = \pm b$, we take following two types of conditions.

Case 1

The boundary is free from tractions, i.e.

$$\sigma_z(\gamma, b, t) = \tau_{\gamma z}(\gamma, b, t) = 0. \tag{8a}$$

Case 2

The slab is confined between rigid planes, i.e.

$$u_z(\gamma, b, t) = u_\gamma(\gamma, b, t) = 0. \tag{8b}$$

3. METHOD OF SOLUTION

We define Laplace transform pair by

$$f^*(p) = \int_0^\infty f(t)\, e^{-pt}\, dt, \qquad f(t) = \frac{1}{2\pi i}\int_{B_\gamma} f^*(p)\, e^{pt}\, dp \tag{9}$$

B_γ represents the Bromwich path.

Now in the Laplace transform plane the eqns (4) and the boundary conditions (5)–(8) becomes

$$\nabla^2 \phi^* = \left(\frac{p}{c_1}\right)^2 \phi^*, \qquad \nabla^2 \psi^* - \frac{\psi^*}{\gamma^2} = \left(\frac{p}{c_2}\right)^2 \psi^* \tag{10}$$

$$\sigma_z^*(\gamma, 0, p) = -\frac{\sigma_0}{p}, \qquad 0 \leqslant \gamma < a \tag{11}$$

$$u_z^*(\gamma, 0, p) = 0, \qquad a < \gamma < \infty \tag{12}$$

$$\tau_{\gamma z}^*(\gamma, 0, p) = 0, \qquad \forall \gamma \tag{13}$$

$$\sigma_z^*(\gamma, b, p) = \tau_{\gamma z}^*(\gamma, b, p) = 0 \tag{14a}$$

$$u_z^*(\gamma, b, p) = \tau_{\gamma z}^*(\gamma, b, p) = 0. \tag{14b}$$

The eqns (10) may be solved with the help of Hankel transform to render

$$\phi^*(\gamma, z, p) = \int_0^\infty [A(s,p)Ch\nu_1 z + B(s,p)Sh\nu_1 z]J_0(s\gamma)\,ds$$

$$\psi^*(\gamma, z, p) = \int_0^\infty [C(s,p)Ch\nu_2 z + D(s,p)Sh\nu_2 z]J_1(s\gamma)\,ds \tag{15}$$

where

$$\nu_j = \left(s^2 + \frac{p^2}{c_j^2}\right)^{1/2}, \qquad j = 1, 2$$

with s-plane being cut such that $\nu_j \geq 0$ for $0 \leq s < \infty$. Applying (13), we get

$$B(s,p) = -\frac{(s^2+\nu_2^2)}{2\nu_1}E(s,p), \qquad c(s,p) = sE(s,p). \tag{16}$$

From conditions (11) and (12) we obtain

$$\int_0^\infty E(s,p)J_0(s\gamma)\,ds = 0, \qquad a < \gamma < \infty \tag{17}$$

$$\int_0^\infty \frac{\{(\nu_2^2+s^2)A(s,p) + 2\nu_2 sD(s,p)\}c_2^2}{p^2(1-K^2)}J_0(s\gamma)\,ds = -\frac{\sigma_0 c_2^2}{p^3(1-K^2)\mu}, \tag{18}$$

$$K^2 = c_2^2/c_1^2, \qquad 0 \leq \gamma < a.$$

Case 1

Applying boundary condition (14a), we get

$$A(s,p) = \frac{\alpha_2}{\alpha_1}E(s,p), \qquad D(s,p) = \frac{\alpha_3}{\alpha_1}E(s,p) \tag{19a}$$

where

$$\alpha_1 = (\nu_2^2+s^2)^2 Sh\nu^2 b \cdot Ch\nu_1 b - 4\nu_1\nu_2 s^2 Ch\nu_2 b \cdot Sh\nu_1 b$$

$$\alpha_2 = 2\nu_2 s^2(s^2+\nu_2^2)(1 - Ch\nu_1 b \cdot Ch\nu_2 b) + \frac{(\nu_2^2+s^2)^3}{2\nu_1}Sh\nu_1 b \cdot Sh\nu_2 b$$

$$\alpha_3 = s(\nu_2^2+s^2)^2(1 - Ch\nu_2 b \cdot Ch\nu_1 b) + 4\nu_1\nu_2 s^3 Sh\nu_2 b \cdot Sh\nu_1 b.$$

Case 2

Boundary condition (14b) gives

$$A(s,p) = \frac{\nu_2^2+s^2}{2\nu_1}\coth \nu_1 b E(s,p), \qquad D(s,p) = -s\coth \nu_2 b E(s,p). \tag{19b}$$

Now with the aid of (19), (18) reduces to

$$\int_0^\infty sF_i(s,p)E(s,p)J_0(sr)\,ds = -\frac{\sigma_0 c_2^2}{p^3(1-K^2)\mu}, \qquad i = 1, 2 \tag{20}$$

where the subscripts 1 and 2 correspond to Case 1 and Case 2 respectively and

$$F_i(s,p) = \frac{\{(s^2+\nu_2^2)\alpha_2 + 2\nu_2\alpha_3 s\}}{\alpha_1 s(1-K^2)}$$

$$F_2(s,p)=\left[\frac{(\nu_2^2+s^2)^2}{2\nu_1 s}\coth \nu_1 b-2\nu_1 s\coth \nu_2 b\right]\frac{c_2^2}{p^2(1-K^2)}.$$

The integral equations (17) is automatically satisfied by taking

$$E(s,p)=-\left(\frac{2sa}{\pi}\right)^{1/2}\frac{c_2^2\sigma_0 a^2}{\mu(1-K^2)p^3}\int_0^1\sqrt{\xi}\phi_i^*(\xi,p)J_{1/2}(sa\xi)\,d\xi,\qquad i=1,2 \tag{21}$$

where ϕ_1^* and ϕ_2^* are unknown functions corresponding to Case 1 and Case 2 respectively. With the help of (21), (20) reduces to

$$\phi_i^*(\xi,p)+\int_0^1\phi_i^*(\eta,p)L_i(\xi,\eta,p)\,d\eta=\xi,\qquad i=1,2 \tag{22}$$

where

$$L_i(\xi,\eta,p)=\frac{2}{\pi}\int_0^\infty\left\{F_i\left(\frac{s}{a},p\right)-1\right\}\sin s\eta\cdot\sin s\xi\,ds,\qquad i=1,2. \tag{23}$$

The values of $\phi_i^*(1,p)$ $(i=1,2)$ are evaluated after solving numerically the integral equations (22) by Fox and Goodwin[5] method. Then $\phi_1^*(1,p)$, $\phi_2^*(1,p)$ as functions of c_2/p_a for different values of $h(=a/b)$ are presented graphically in Figs. 1 and 2. They are used subsequently for determining the dynamic stress intensity factor.

4. NUMERICAL DISCUSSIONS

Numerical computations are carried out on IBM 370/155 computer at the Computer Centre I.I.T., Madras. The Fredholm integral equation (22) is solved numerically by Fox and Goodwin[5] method and the values of $\phi_i^*(\xi,p)$ $(i=1,2)$ are obtained at discrete points of c_2/pa and $\xi=0.1,0.2,\ldots,1.0$. The graphs of $\phi_i^*(1,p)$ $(i=1,2)$ vs c_2/pa are presented in two graphs for different values of h. Then numerical Laplace inversion technique developed by Miller and Guy[6] is used to obtain the dynamic stress-intensity factor at the crack tips.

5. CONCLUSION

Figures 1 and 2 show the variations of $\phi_i^*(1,p)$ $(i=1,2)$ vs c_2/pa. From these figures it is observed that for the slab having stress free edge the values are more in comparison to the infinite medium, where as for slab confined between two rigid planes it is just opposite. Figures

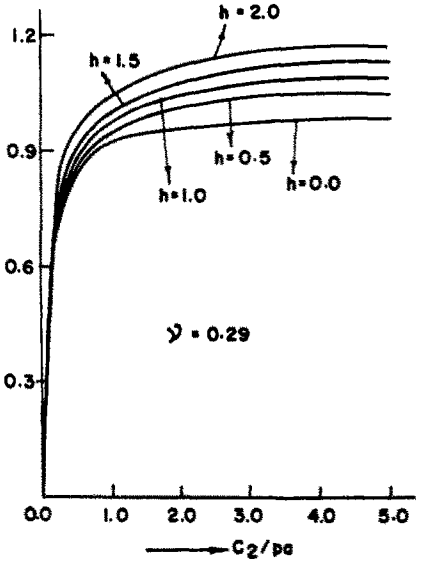

Fig. 1. Variation of $\phi_1^*(1,p)$ vs c_2/pa for the case when the edge of the slab is stress free

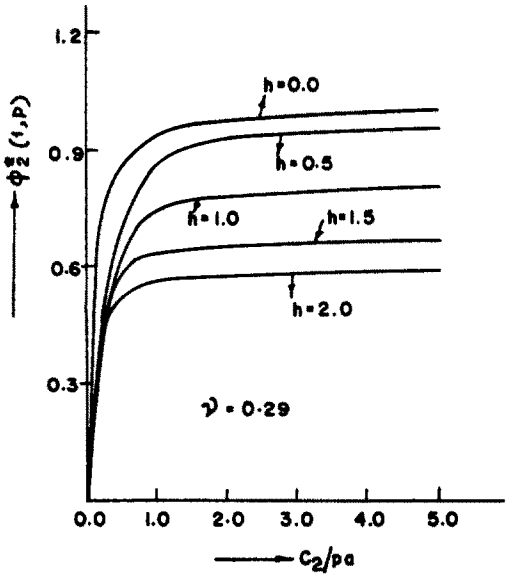

Fig. 2. Variation of $\phi^*(1, p)$ vs c_2/pa for the case when the slab is confined between two rigid planes.

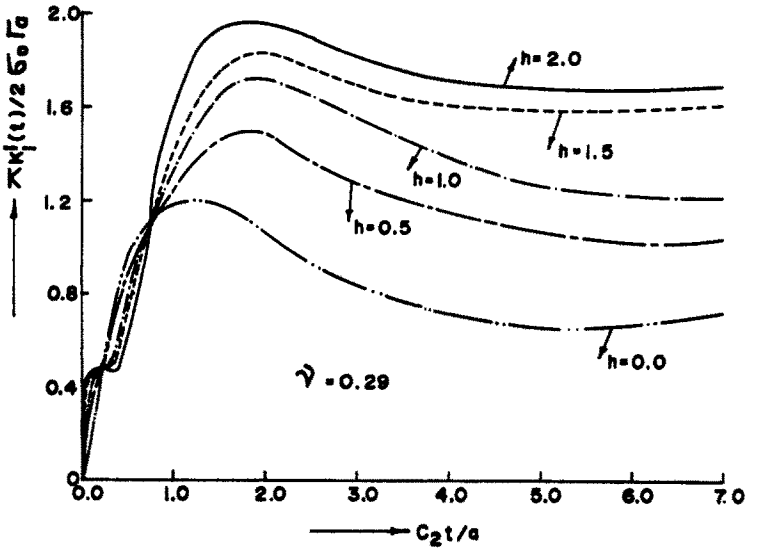

Fig. 3. Variation of dynamic stress-intensity factor with time, for the stress free boundary.

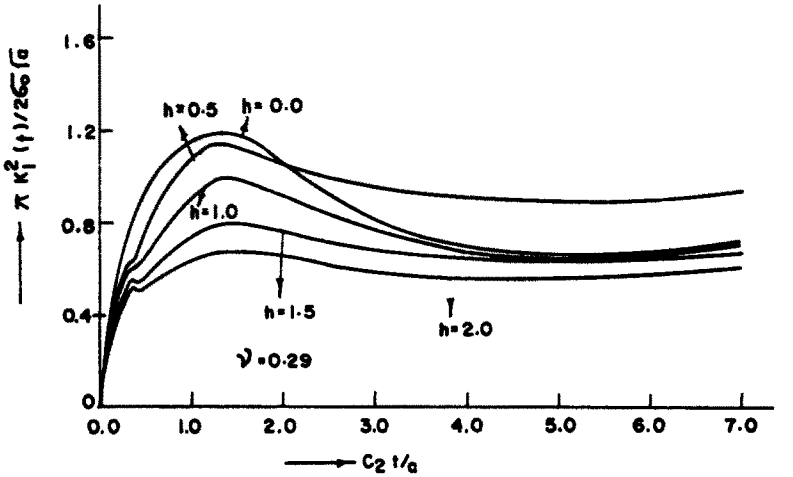

Fig. 4. Variation of dynamic stress-intensity factor with time, for the slab, confined between two rigid planes.

Table 1. Comparison between the static and maximum dynamic stress-intensity factors

h	0.0	0.5	1.0	1.5	2.0
K_1^{1m}	1.19	1.53	1.82	1.90	1.91
K_1^{1s}	0.74	1.02	1.23	1.62	1.75
K_1^{2m}	1.19	1.11	0.97	0.782	0.668
K_1^{2s}	0.74	0.957	0.72	0.702	0.632

3 and 4 depict the variations of normalised dynamic stress-intensity factors ($\pi K_1^1(t)/2\sigma_0\sqrt{a}$ and $\pi K_1^2(t)/2\sigma_0\sqrt{a}$) vs c_2t/a for $\nu = 0.29$ and for different values of h (0.5, 1.0, 1.5, 2.0) and are compared with that of infinite medium [7]. The general feature which can be noticed from these graphs is that the stress-intensity factor rise rapidly with time reaching a peak, then decreases in magnitude and oscillates about its corresponding static value. For stress free boundary (Fig. 3) the peak value increases with h, where as for the slab confined between two rigid planes the peak value decreases as h increases. In Fig. 4, the curves for $h = 0.0 \wedge h = 0.5$ intersect each other for $c_2t/a = 2.0$. The curves are somewhat disturbed in the intervals $0.2 \leq c_2t/a \leq 0.5$ (Fig. 3), $0.3 \leq c_2t/a \leq 0.6$ (Fig. 4). It is interesting to note that these regions may correspond to the first arrival of the reflected longitudinal and shear waves at the crack tips from the boundary. Another interesting point is that when "t" is very large the problem reduces to the static case. It is observed that the static stress-intensity factor for every h is less than the maximum dynamic stress-intensity factor (for both the cases). The above comparison is given in Table 1.

In the figures $K_1^1(t)$ and $K_1^2(t)$ represent dynamic stress-intensity factors for Case I and Case II respectively.

In Table 1, K_1^{1m}, K_1^{1s} and K_1^{2m}, K_1^{2s} represent maximum dynamic stress-intensity factor and static stress-intensity factor for Case 1 and Case 2 respectively.

REFERENCES

1. G. C. Sih and J. F. Loeber, Normal compression and radial shear waves scattering at a penny-shaped crack in an elastic solid. *J. Accoust. Soc. Am.* **46**(3), 711 (1969).
2. G. T. Embley and G. C. Sih, Response of a penny-shaped crack to impact waves. *Development in Mechanics* **6**, 473 (1971).
3. G. C. Sih and G. T. Embley, Sudden twisting of a penny-shaped crack. *J. Appl. Mech.* **39**, 395 (1971).
4. E. P. Chen, Elastodynamic response of a penny-shaped crack in a cylinder of finite radius. *Int. J. Engng Sci.* **17**, 379 (1979).
5. L. Fox and E. T. Goodwin, The numerical solution of non-singular linear integral equations. *Phil. Trans. R. Soc.* **A245**, 501 (1953).
6. M. K. Miller and W. T. Guy, Numerical inversion of the Laplace transform by use of Jacobi polynomials. *SIAM J. Numer. Anal.* 3, 624 (1966).
7. E. P. Chen and G. C. Sih, *Elastodynamic Crack Problems*. Noordhoff, Leyden (1977).